Small-angle neutron scattering study of differences in phase behavior of silica nanoparticles in the presence of lysozyme and bovine serum albumin proteins

Indresh Yadav,[1] Sugam Kumar,[1] V. K. Aswal,[1] and J. Kohlbrecher[2]
[1]*Solid State Physics Division, Bhabha Atomic Research Centre, Mumbai 400 085, India*
[2]*Laboratory for Neutron Scattering, Paul Scherrer Institut, CH-5232 PSI Villigen, Switzerland*
(Received 6 November 2013; published 10 March 2014)

The differences in phase behavior of anionic silica nanoparticles (88 Å) in the presence of two globular proteins [cationic lysozyme (molecular weight (MW) 14.7 kD) and anionic bovine serum albumin (BSA) (MW 66.4 kD)] have been studied by small-angle neutron scattering. The measurements were carried out on a fixed concentration (1 wt %) of Ludox silica nanoparticles with varying concentrations of proteins (0–5 wt %) at $p\mathrm{H} = 7$. It is found that, despite having different natures (opposite charges), both proteins can render to the same kind of aggregation of silica nanoparticles. However, the concentration regions over which the aggregation is observed are widely different for the two proteins. Lysozyme with very small amounts (e.g., 0.01 wt %) leads to the aggregation of silica nanoparticles. On the other hand, silica nanoparticles coexist with BSA as independent entities at low protein concentrations and turn to aggregates at high protein concentrations (>1 wt %). In the case of lysozyme, the charge neutralization by the protein on the nanoparticles gives rise to the protein-mediated aggregation of the nanoparticles. The nanoparticle aggregates coexist with unaggregated nanoparticles at low protein concentrations, whereas, they coexist with a free protein at higher protein concentrations. For BSA, the nonadsorbing nature of the protein produces the depletion force that causes the aggregation of the nanoparticles at higher protein concentrations. The evolution of the interaction is modeled by the two Yukawa potential, taking account of both attractive and repulsive terms of the interaction in these systems. The nanoparticle aggregation is found to be governed by the short-range attraction for lysozyme and the long-range attraction for BSA. The aggregates are characterized by the diffusion limited aggregate type of mass fractal morphology.

DOI: 10.1103/PhysRevE.89.032304 PACS number(s): 82.70.Dd, 87.14.E−, 61.46.−w, 61.05.fg

I. INTRODUCTION

There is a lot of current interest in nanotechnology for industrial applications in optoelectronics, information technology, bionanotechnology, and medicine, to name but a few [1–5]. Due to their large surface area and quantum confinement, nanoparticles display many useful properties (mechanical, electrical, magnetic, optical, etc.) from those of their constituent atoms and bulk materials. These properties are size dependent and can be tuned depending on the requirement [1,6–8]. In particular, the nanoparticles, being small, can interact with cellular machinery in biological applications. For example, nanoparticle-protein systems are extensively utilized in drug delivery, catalysis, biological imaging, biosensors, and biofuel cells [9–13].

Engineered nanoparticles have a great impact on the environment and biological functioning of all the living. The environmental biomolecules (e.g., natural organic materials, proteins, and detergents) have a tendency to cover the nanoparticle as nanoparticles have very high surface energies, which results in forming new entities of biomolecules around the nanoparticle and is called the biological corona [9,14,15]. The formation and function of this biological corona strongly depend on the nature of both the nanoparticle and the biomolecule. The functional property of biomolecules may change when they come in contact with nanoparticles. This, in turn, is also important for the colloidal stability of the nanoparticles and their resultant structures [16]. Therefore, understanding of the nanoparticle-biomolecule complex is important for the safe and beneficial use of nanoparticles [17].

Colloidal dispersions of inorganic nanoparticles in the matrices of proteins show rich phase behavior by providing a model system to study the interaction of nanoparticles with biomolecules [18,19]. The intrinsic characteristic of the nanoparticles (e.g., size, shape, and charge) and the forces (e.g., electrostatic, hydrogen bonding, and steric forces) at the bionanointerface control the phase behavior, which can be tuned by varying different solution parameters, such as ionic strength, pH, temperature, and concentration [17,20,21]. There have been a number of studies on the interaction of lysozyme and bovine serum albumin (BSA) proteins with different inorganic nanoparticles [22–26]. Silica nanoparticles are one of the most commonly used model inorganic nanoparticles, which are nontoxic and biocompatible as well as less expensive and commercially available [27]. The globular proteins (e.g., BSA and lysozyme) are known to be highly stable, available with high purity, and easily soluble in water. It has been found that, for charged stabilized nanoparticles, the electrostatic interaction between nanoparticle and protein govern their phase behaviors [28]. The adsorption of the cationic lysozyme on the surface of anionic silica nanoparticles leads to the protein-mediated aggregation of the nanoparticles [29]. On the other hand, despite BSA and silica nanoparticles having similar charges (both are anionic), site-specific adsorption of BSA on silica nanoparticles has been reported [30]. The formation of the core-shell structure as a consequence of adsorption of BSA on a silica surface is believed unlikely to favor any kind of nanoparticle aggregates [31].

Herein, we have examined the differences in the interaction and structural evolution of colloidal silica nanoparticles for their interaction over a wide range of concentrations of lysozyme and BSA proteins at physiological conditions. Although the different phase behaviors of anionic silica nanoparticles with cationic lysozyme and anionic BSA are

 ©2014 American Physical Society

expected because of the differences in their electrostatic interaction, they (silica nanoparticle-lysozyme protein and silica nanoparticle-BSA protein) interestingly show similar behaviors at very low and high protein concentrations. These systems have been characterized by small-angle neutron scattering (SANS), which is a powerful technique to study such multicomponent systems [32,33]. SANS gives the scattering patterns in Fourier space form where the real space sample information is obtained by fitting experimental data using a suitable model. Both the structure and the interaction can be obtained using this method in *in situ* and under native environments [34–37].

II. EXPERIMENTS

Spherical silica nanoparticles (Ludox HS-40), hen egg lysozyme, and BSA proteins were purchased from Sigma-Aldrich. Electrostatically stabilized Ludox silica nanoparticles were received as dispersed colloidal particles having 40 wt % concentration in water and proteins in powder form. Samples were prepared by dissolving the weighted amount of nanoparticles and proteins in a 20 mM phosphate buffer at pH = 7 prepared in D_2O. Samples for neutron scattering experiments are prepared in D_2O instead of H_2O because of the high contrast for the hydrogenous sample in D_2O. Small-angle neutron scattering experiments were performed on the SANS-I instrument at the Swiss spallation neutron source, SINQ, Paul Scherrer Institut, Switzerland [38]. The mean wavelength (λ) of the incident neutron beam was 6 Å with the wavelength resolution of approximately 10%. The scattered neutrons were detected by using a 96 × 96 cm^2 detector. The experiments were performed at two sample-to-detector distances of 2 and 8 m, respectively, to cover the data in the scattering vector [$Q = 4\pi \sin(\theta/2)/\lambda$, where θ is the scattering angle] range of 0.006–0.25 $Å^{-1}$. All the measurements were carried out for a fixed concentration (1 wt %) of silica nanoparticles and varying the concentration of proteins in the range of 0–5 wt %. The freshly prepared samples were held in Hellma quartz cells having thicknesses of 2 mm, and temperatures were kept constant at 30 °C during the measurements. The data were corrected and were normalized at absolute scale using a standard procedure.

III. SMALL-ANGLE NEUTRON SCATTERING ANALYSIS

In the SANS experiment, the coherent differential scattering cross section per unit volume ($d\Sigma/d\Omega$) is measured as a function of scattering vector Q. In the case of monodisperse particles (nanoparticles or protein macromolecules) dispersed in a medium, it can be written as [39,40]

$$\frac{d\Sigma}{d\Omega}(Q) = nV^2(\rho_p - \rho_s)^2 P(Q)S(Q) + B, \tag{1}$$

where n is the number density and V is the particle volume. ρ_p and ρ_s are scattering length densities of particles and solvents, respectively. $P(Q)$ is the intraparticle structure factor, and $S(Q)$ is the interparticle structure factor. B is a constant term representing incoherent background.

$P(Q)$ depends on the shape and size of the particle and is the square of the single particle form factor $F(Q)$ as given by

$$P(Q) = \langle |F(Q)|^2 \rangle. \tag{2}$$

For a spherical particle of radius R, $F(Q)$ is expressed as

$$F(Q) = \frac{3\{\sin(QR) - QR\cos(QR)\}}{(QR)^3}. \tag{3}$$

In the case of an ellipsoidal particle, $P(Q)$ is given by

$$P(Q) = \int_0^1 [F(Q,\mu)^2 d\mu] \tag{4}$$

$$F(Q,\mu) = \frac{3(\sin x - x\ \cos x)}{x^3}, \qquad x = Q[a^2\mu^2 + b^2(1-\mu^2)]^{1/2}, \tag{5}$$

where a and b are the semimajor and semiminor axes, respectively, of the ellipsoidal particle and μ is the cosine of the angle between the directions of a and the wave vector transfer Q.

$S(Q)$ correlates particles present in the system and gives information about the interactions in the system. For dilute systems, $S(Q) \sim 1$. The scattering from the system having two noninteracting components (e.g., nanoparticle and protein) can be modeled by summing the two contributions from individual components as given by [41]

$$\left(\frac{d\Sigma}{d\Omega}\right)(Q) = \left(\frac{d\Sigma}{d\Omega}\right)_n(Q) + \left(\frac{d\Sigma}{d\Omega}\right)_p(Q), \tag{6}$$

where n and p denote the nanoparticle and protein contributions, respectively.

For an isotropic system, $S(Q)$ can be written as

$$S(Q) = 1 + 4\pi n \int [g(r) - 1]\frac{\sin\ Qr}{Qr} r^2 dr, \tag{7}$$

where $g(r)$ is the radial distribution function. It is the probability of finding the particle at a distance r from a reference particle centered at the origin. The $g(r)$ is governed by the form of the potential $V(r)$. The evolution of the interaction between nanoparticles on the addition of the protein has been calculated using the two Yukawa (2Y) potential under mean spherical approximation [42,43]. The 2Y potential, having four dimensionless parameters (K_1, K_2, Z_1, and Z_2), is expressed by

$$\frac{V(r)}{k_BT} = \infty \quad (r \leqslant \sigma) \qquad = V_{2Y}/k_BT \quad (r > \sigma), \tag{8}$$

where

$$\frac{V_{2Y}(r)}{k_BT} = -K_1\frac{\exp[-Z_1(r/\sigma - 1)]}{r/\sigma} + K_2\frac{\exp[-Z_2(r/\sigma - 1)]}{r/\sigma}, \tag{9}$$

and σ is the hard sphere diameter of the nanoparticle.

In the case of particle aggregation as characterized by fractal structure, the scattering cross section can be expressed as [44]

$$\frac{d\Sigma}{d\Omega}(Q) = n_a V_p^2(\rho_p - \rho_s)^2 P(Q)S_f(Q) + B, \tag{10}$$

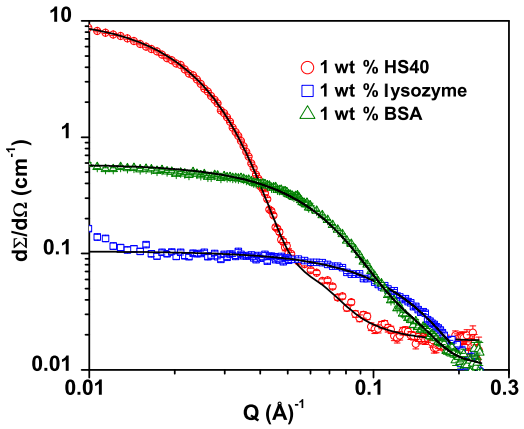

FIG. 1. (Color online) SANS data from 1 wt % of HS40 silica nanoparticles, lysozyme, and BSA proteins in aqueous solution.

where n_a and V_p are the number density and volume of the individual scatterer in the aggregates. $P(Q)$ is the intraparticle structure factor of the building block in the aggregated structures. The static structure factor $S_f(Q)$ for the mass fractal is given by

$$S_f(Q) = 1 + \frac{1}{(QR)^D} \frac{D\Gamma(D-1)}{\left[1+\frac{1}{(Q\xi)^2}\right]^{(D-1)/2}} \times \sin\{(D-1)\tan^{-1}(Q\xi)\}, \quad (11)$$

where ξ signifies the maximum length up to which fractal microstructure exists, R is the size of the building block, and D is the fractal dimension. Γ is the mathematical γ function.

For a polydisperse system, the differential scattering cross section can be written as [45]

$$\frac{d\Sigma}{d\Omega}(Q) = \int \frac{d\Sigma}{d\Omega}(Q,R) f(R) dR + B, \quad (12)$$

where $f(R)$ is the size distribution that incorporates the polydispersity of the particles and usually is accounted for by the log-normal distribution as given by the following expression:

$$f(R) = \frac{1}{R\sigma\sqrt{2\pi}} \exp\left[-\frac{\left(\ln\frac{R}{R_{\rm med}}\right)^2}{2\sigma^2}\right], \quad (13)$$

where $R_{\rm med}$ and σ are the median value and standard deviation (also referred to as polydispersity), respectively. The mean R_m and median values are related as $R_m = R_{\rm med}\exp(\frac{\sigma^2}{2})$. The integration in Eq. (12) is carried out over $P(Q)$ for simplification, whereas, $S(Q)$ is calculated for the mean size of the particle.

Throughout the data, analysis corrections were made for instrumental smearing where calculated scattering profiles are smeared by the appropriate resolution function to compare with the measured data. The parameters in the analysis were optimized by means of the nonlinear least-squares fitting program [46].

IV. RESULTS AND DISCUSSION

Figure 1 shows the SANS data from HS40 silica nanoparticles, lysozyme, and BSA proteins (1 wt % each) in aqueous solution. All the data show a monotonically decreasing profile as a function of scattering vector Q. At the concentration of 1 wt %, the interaction between the nanoparticles (or proteins) can be neglected, i.e., $S(Q) \sim 1$. Hence, the scattering is predominantly governed by the form factor of the scatterers [41,47]. Fitted parameters of silica nanoparticles and proteins are given in Table I. A polydisperse spherical model combining Eqs. (3) and (12) is used to fit the scattering profile of the silica nanoparticles. The mean radius of the silica nanoparticles is found to be 88.0 Å with a polydispersity of 0.2. Both lysozyme and BSA proteins are known to have globular structures and, hence, have been fitted with ellipsoidal shapes using Eq. (1). Lysozyme data are best fitted with prolate ellipsoidals having semimajor and semiminor axes of 24.0 and 13.5 Å, respectively. On the other hand, BSA has an oblate ellipsoidal shape with semimajor and semiminor axes of 42.0 and 15.0 Å, respectively. There is the possibility of the existence of some permanent aggregates in the proteins which could be responsible for scattering buildup at low Q as seen in the case of lysozyme [48]. The significantly larger size of the nanoparticles (R_m = 88 Å) than those of the proteins (R_e = 16.3 Å for lysozyme and 29.8 Å for BSA) has been chosen from the point of view that there is enough adsorption of proteins on the nanoparticles, if any.

Figure 2 shows the phase behavior of 1 wt % of HS40 silica nanoparticles with varying concentrations of lysozyme and BSA. The figure depicts the variation in the transmission of light (6000 Å) of a silica nanoparticle system as a function of protein concentration. These measurements were also carried out on D_2O to be able to perform the direct comparison of phase behavior with the SANS results. It is known that proteins in

TABLE I. Fitted parameters of 1 wt % of HS40 silica nanoparticles, lysozyme, and BSA proteins in aqueous solution.

(a) HS40 silica nanoparticles

Sample	Mean radius R_m (Å)	Polydispersity (σ)
1 wt % HS40	88.0	0.20

(b) Lysozyme and BSA proteins

Sample	Shape	Semimajor axis a (Å)	Semiminor axis b (Å)	Equivalent radius R_e (Å)
1 wt % lysozyme	Prolate ellipsoidal	24.0	13.5	16.3
1 wt % BSA	Oblate ellipsoidal	42.0	15.0	29.8

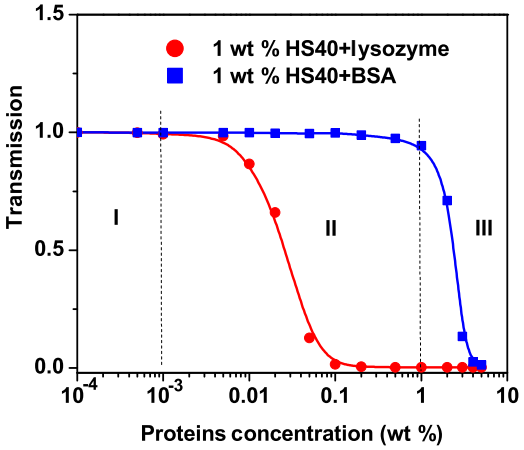

FIG. 2. (Color online) Transmission of light in 1 wt % of HS40 silica nanoparticles with varying concentrations of lysozyme and BSA proteins.

D_2O, as compared to H_2O, may behave differently (e.g., have a higher tendency to aggregate) [49]. The transmission of light depends on the evolution of the structure in the system where the formation of larger structures will scatter more light and, hence, the decrease in the transmission. It is observed that the value of transmission decreases dramatically beyond a critical concentration for both proteins. It is interesting to note that, despite having a repulsive interaction between nanoparticle and BSA, they show a similar behavior as that of an attractive interaction between nanoparticle and lysozyme. The critical concentration is very different for lysozyme and BSA, almost three orders higher in the case of BSA. The comparison of phase behavior for the two proteins can be divided in three concentration-dependent regions. The first region corresponds to the very low protein concentrations (<0.001 wt %) where silica nanoparticles with both lysozyme and BSA have high transmissions corresponding to the systems having similar structures of nanoparticles without and with proteins. All the systems form a clear solution in this region. In the second region of intermediate protein concentration (0.001–1 wt %), the transmission of lysozyme decreases and becomes very low, whereas, transmission with BSA remains unchanged. The decrease in the transmission with lysozyme is expected if the nanoparticles aggregate in the presence of lysozyme. This system is also observed to be turbid in this region. In the last (third) region (>1 wt %), BSA also shows low transmission (becomes turbid) similar to that observed with

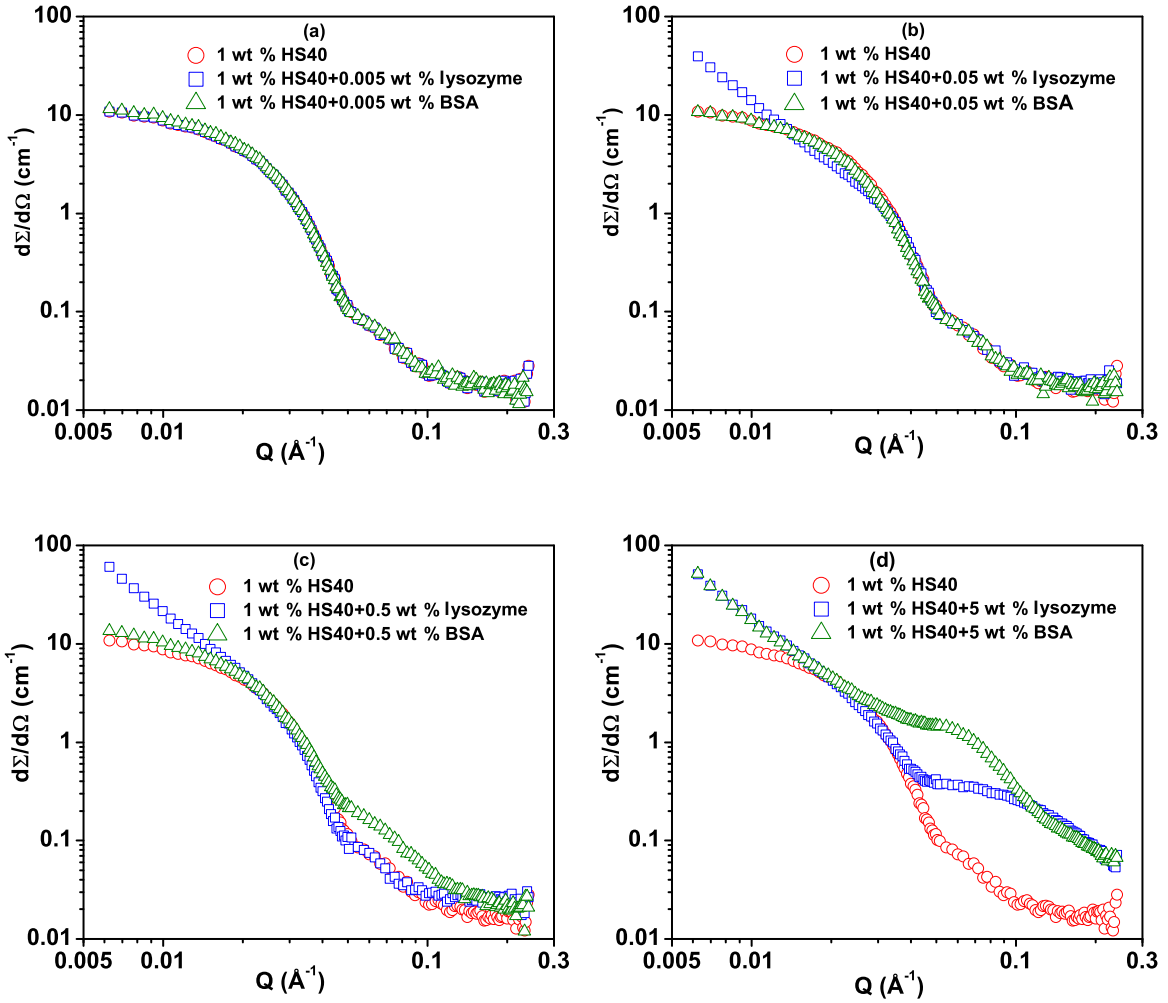

FIG. 3. (Color online) SANS data of 1 wt % of HS40 silica nanoparticles with (a) 0.005 wt %, (b) 0.05 wt %, (c) 0.5 wt %, and (d) 5 wt % of lysozyme and BSA concentrations.

lysozyme. This suggests both proteins show a similar phase behavior of structural evolution despite the difference in the electrostatic interaction (attraction vs repulsion) of the two proteins with the nanoparticles. However, the concentration range over which the structural evolution is observed and, more importantly, the mechanism leading to the similar phase behavior is very different. SANS measurements have been carried out to understand the mechanism for the interaction of silica nanoparticles with lysozyme and BSA proteins.

The SANS data from 1 wt % of HS40 silica nanoparticles with lysozyme and BSA proteins in the different regions of their phase behavior (Fig. 2) are compared in Fig. 3. In region I of the phase behavior, at very low protein concentrations, the SANS data in the presence of both protein systems overlap that of the pure silica nanoparticles system [Fig. 3(a)]. This region (region I) represents where the number density of proteins is very low, and therefore, their interaction (lysozyme and BSA), if any, with the nanoparticles seems negligible. For region II, silica nanoparticles with lysozyme and BSA behave very differently, which is also reflected in the SANS data [Figs. 3(b) and 3(c)]. The data of BSA in region II are similar to that in region I, which is an indication of no significant interaction of BSA with nanoparticles observed even up to 0.5 wt % concentration of BSA. In the low Q, the scattering is dominated by the individual nanoparticles, whereas, at high Q, the scattering from the noninteracting protein becomes visible with the increase in protein concentration [Fig. 3(c)]. Unlike the case of BSA, the lysozyme data show a strong scattering buildup in the low Q; such scattering is usually seen for aggregated particles [50,51]. These aggregates are believed to be responsible for the decrease in the transmission of the nanoparticle-lysozyme system in region II. In region III, the presence of both BSA and lysozyme make the nanoparticles system turbid. The SANS data of BSA in this region (region III) are found to be similar to that as observed for lysozyme in region II [Fig. 3(d)]. The low Q data for both proteins suggest similar aggregation in these systems, whereas, the difference at high Q arises because of the difference in the sizes of the two proteins. Because lysozyme and BSA are oppositely charged, we expect their different interactions with the nanoparticle are responsible for the similar behavior of the nanoparticles in region III.

To understand the evolution of the interaction and structure of silica nanoparticles in the presence of lysozyme, the scattering profiles of 1 wt % of silica nanoparticles with varying concentrations (0–5 wt %) of the lysozyme protein are shown in Fig. 4. Based on the features of scattering data, these have been divided into three groups: (a) a low protein concentration (0.0–0.02 wt %) group [Fig. 4(a)] where the system goes from region I to region II of the phase behavior and the remaining two groups corresponding to region II for the intermediate protein concentration (0.05–0.2 wt %) group [Fig. 4(b)] and the higher protein concentration (0.5–5 wt %) group [Fig. 4(c)]. Figure 4(a) shows that adding small amounts of lysozyme with silica nanoparticles gives a scattering buildup in the low Q and the system moves from region I to region II. It is also seen that there is no significant change in the scattering profiles except in the low Q. The scattering buildup in the low Q arises due to a change in interaction between nanoparticles and/or by the evolution of a structure, such as the formation of aggregates in the presence of

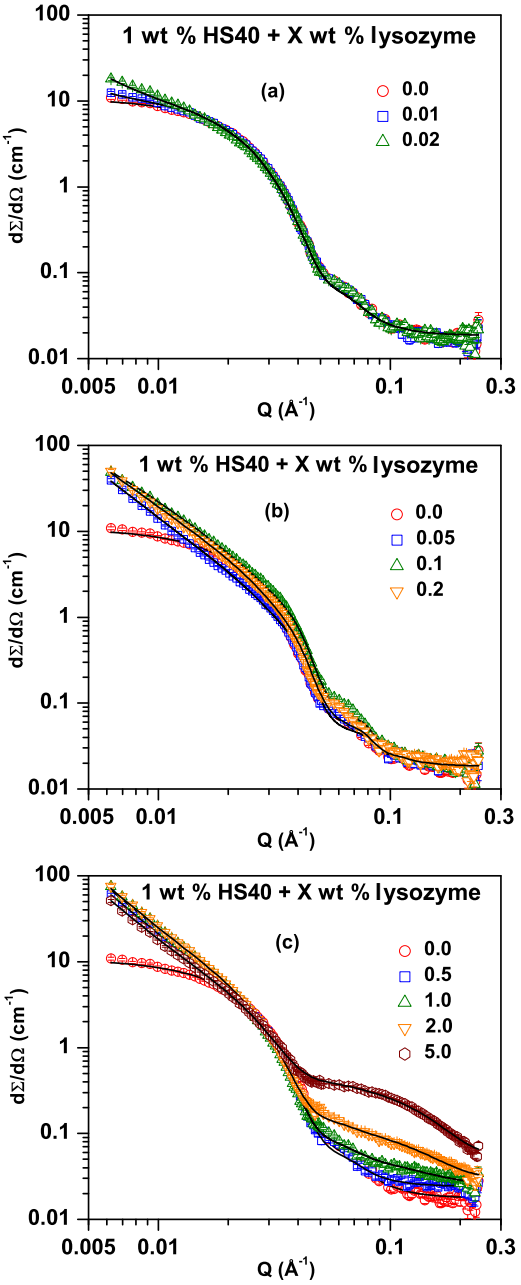

FIG. 4. (Color online) SANS data of 1 wt % of HS40 silica nanoparticles with lysozyme protein (a) low concentration (0.0–0.02 wt %), (b) intermediate concentration (0.05–0.2 wt %), and (c) high concentration (0.5–5 wt %).

lysozyme [29,43,47]. At the physiological condition (pH = 7), silica nanoparticles and lysozyme are oppositely charged, and as a result, lysozyme adsorbs on the surface of the silica nanoparticles and, hence, mediates in an attractive interaction between nanoparticles and their aggregation [29,47]. The data are, therefore, fitted considering nanoparticles undergoing attractive interaction and coexisting with the aggregates of the nanoparticles. Because the nanoparticle-protein system becomes turbid, even with the small amount 0.01 wt % of lysozyme, the data in Fig. 4(a) are fitted with some nanoparticle aggregates coexisting with unaggregated nanoparticles. With increasing the concentration of lysozyme, the linearity of

TABLE II. Fitted parameters of 1 wt % of HS40 + X wt % of lysozyme.

(a) Low protein concentration regime where the nanoparticle aggregates coexist with noninteracting unaggregated nanoparticles.

Concentration C (wt %)	Fractal dimension D	Building block radius R_b (Å)	Fraction of unaggregated nanoparticles ϕ_{unp} (%)
0.0		90.0	100
0.01	2.5	90.2	90
0.02	2.4	91.3	70

(b) Intermediate protein concentration regime where the nanoparticle aggregates coexist with the interacting unaggregated nanoparticles. The fractal dimension of the nanoparticle aggregates $D = 2.4$ and parameters of the repulsive interaction $K_2 = 9.0$ and $Z_2 = 7.0$ were kept fixed.

Concentration C (wt %)	Building block radius R_b (Å)	K_1	Z_1	Fraction of unaggregated nanoparticles ϕ_{unp} (%)
0.05	90.0	26.5	10.0	40
0.1	94.5	29.5	13.0	30
0.2	93.2	40.0	14.5	10

(c) High protein concentration regime where the nanoparticle aggregates coexist with excess free proteins.

Concentration C (wt %)	Fractal dimension D	Building block radius R_b (Å)	Fraction of free protein ϕ_{fp} (%)
0.5	2.4	94.2	
1.0	2.5	95.2	35
2.0	2.4	93.1	70
5.0	2.4	94.0	85

scattering increases at the low Q range without affecting the high Q range [Fig. 4(b)]. The linearity at low Q on the log-log scale suggests that the aggregates' structure could be fractal [47,52]. Fractal aggregates along with some particles interacting with the two Yukuwa potential [Eq. (8)] have been used to fit the scattering profile for lysozyme concentration (0.05–0.2 wt %) giving a signature for the existence of short-range attractive interaction in the system. As the lysozyme concentration is not enough to bind every particle in the fractal structure, the remaining particles form flocculates interacting via oppositely charged protein-mediated short-range attractive interaction between nanoparticles. For protein concentration (0.5–5 wt %), as shown in Fig. 4(c), all the nanoparticles have undergone fractal aggregation. The scattering hump at higher Q values suggests the excess protein coexisting with the nanoparticle aggregates [47]. Thus, the strong electrostatic attractive interaction in the case of silica nanoparticles with lysozyme proteins leads to the protein-mediated aggregation of nanoparticles irrespective of the protein concentration used. The fractal dimension is found to be about 2.4 in all these systems. The fitted parameters are given in Table II. The observations of phase behavior in Fig. 2 are found to be consistent with that of the SANS results in Fig. 4. The decrease in light transmission for lysozyme in moving from region I to region II in Fig. 2 follows the increase in the calculated volume fraction of the aggregated nanoparticles (Table II).

The protein-mediated interaction between nanoparticles is fitted using the 2Y potential comprising four fitting parameters (K_1,K_2,Z_1,Z_2). Here, K_1 and Z_1 are the fitting parameters of the attractive potential to give the strength (proportional to K_1) and range (proportional to $1/Z_1$), respectively [36,43]. On the other hand, K_2 and Z_2 are the fitting parameters of the repulsive potential, which provides the strength (related to effective charge) and range (related to ionic strength), respectively [51]. The parameters of the repulsive potential have been determined from the pure concentrated solution of the nanoparticles as

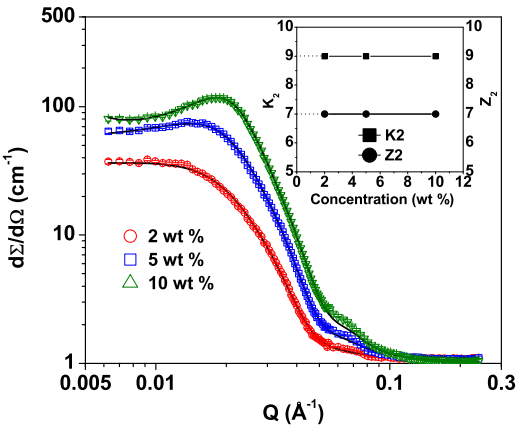

FIG. 5. (Color online) SANS data of HS40 silica nanoparticles with varying concentrations. The inset shows the values of K_2 and Z_2 obtained by fitting the SANS data.

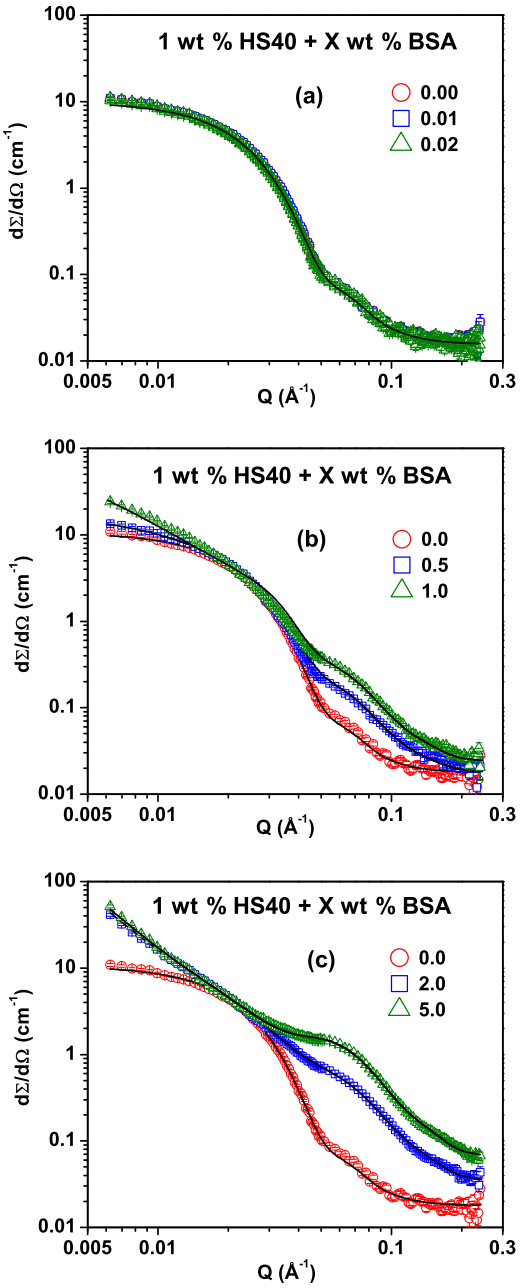

FIG. 6. (Color online) SANS data of 1 wt % of HS40 silica nanoparticles on addition with BSA protein having (a) low concentration (0.01–0.2 wt %), (b) intermediate concentration (0.5–1 wt %), and (c) high concentration (2–5 wt %).

it is difficult to see the $S(Q)$ contribution from the repulsive interaction in 1 wt % or lower concentration of the nanoparticle system. The SANS data are taken at different concentrations (Fig. 5), and the parameters for 1 wt % are obtained by the extrapolation of the fitted parameters of higher concentrations (inset of Fig. 5). These parameters' repulsive interactions are fixed in the analysis of the SANS data, and the parameters of the attractive interaction are obtained as only fitted parameters. It is found that, unlike long-range repulsion, the attractive interaction is short range. It seems to be governed by the distance over which the protein is effectively mediating the attractive interaction between two nanoparticles. The short range arises as a result of nonuniform charge distribution on the protein, which makes it highly site specific to mediate between oppositely charged nanoparticles.

SANS profiles of the silica nanoparticle-BSA system are shown in Fig. 6. Data similar to those of silica nanoparticle lysozyme are divided in three groups of protein concentrations. First, the low concentration group (0.0–0.2 wt %) [Fig. 6(a)] is corresponding to regions I and II of the phase behavior (Fig. 2) where the system remains transparent. The second group's data [Fig. 6(b)] are from the intermediate concentration range (0.5–1 wt %) corresponding to transition regions II to III of the phase behavior. The third (2–5 wt %) group [Fig. 6(c)] for high protein concentrations corresponds to region III of the phase behavior where the system becomes turbid. It is observed that the silica nanoparticle-BSA data have very different features than the silica nanoparticle lysozyme. Figure 6(a) shows no significant change in SANS data of 1 wt % of silica nanoparticles on the addition of the BSA protein up to 0.2 wt % concentration. Data of the silica nanoparticle-BSA system are similar to that of pure silica nanoparticles. There is no indication of any large structure in the system by SANS, and the system is seen to be transparent. The scattering is dominated by that of the silica nanoparticles. Data were fitted by considering the scattering contributions from the individual nanoparticles and the free protein using Eq. (6). That is unlike the silica nanoparticle lysozyme, and the nanoparticles and protein in silica nanoparticle BSA remain as individual entities in the solvent. There is the possibility that the site-specific adsorption of BSA on the silica surface can take place to form a protein corona (core-shell structure) [53,54] but is not supported by the SANS analysis. Thus, it is clear that electrostatic repulsion prevents any kind of protein adsorption on the nanoparticles since both components are similarly charged. There could be another kind of force in the system, for example, entropic force (depletion, etc.) whose effect is not visible in the SANS data as the concentration of BSA may not be enough. As the concentration of BSA protein increases ($\geq$0.5 wt %), buildup in scattering intensity starts at low Q as well as at high Q regions [Fig. 6(b)]. In this case, the scattering buildup at low Q, unlike the silica nanoparticle-lysozyme system, cannot be attributed to some structural evolution (aggregates). This is because the phase behavior is not consistent with the formation of the aggregates as the transmission of the silica nanoparticle-BSA system does not decrease in the concentration range of the protein. We expect some interactional changes in the system responsible for scattering buildup at lower Q. Scattering data in Fig. 6(b) have been modeled by the 2Y potential [Eq. (8)]. Fitted parameters

TABLE III. Fitted parameters of 1 wt % of HS40 + X wt % of BSA in the intermediate protein concentration regime where the nanoparticles experience depletion interaction prior to their aggregation. The parameters of the repulsive interaction $K_2 = 9.0$ and $Z_2 = 7.0$ were kept fixed.

Concentration C (wt %)	K_1	Z_1
0.5	10.5	4.0
1.0	26.5	3.0

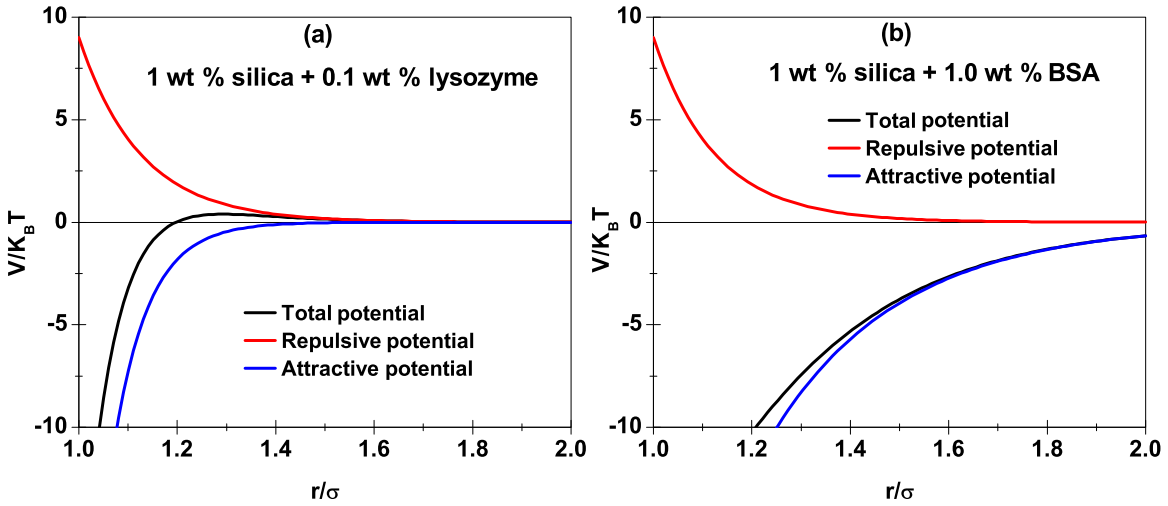

FIG. 7. (Color online) The calculated interaction potentials responsible for the aggregation of silica nanoparticles in the presence of (a) lysozyme and (b) BSA proteins.

are given in Table III. In this case, the attractive potential is found to be relatively long range [50]. The silica nanoparticle-BSA system becomes turbid at higher BSA concentrations (2–5 wt %) as shown in region III of the phase behavior. SANS data show linearity on the log-log scale at low Q, like the silica nanoparticle-lysozyme system [Fig. 4(c)]. We believe nonadsorption of BSA leads to depletion induced aggregation of the nanoparticles. The aggregate size in such a case is known to depend on the depletant (BSA protein) concentration and increases with increases in concentration [50], which could give the difference in the light transmission as observed for 2 and 5 wt % of BSA in Fig. 2. The aggregate sizes are expected to be much larger than can be determined in the present Q range ($2\pi/Q_{\min} \sim 1000$ Å) of the SANS measurements. This may be the reason that SANS data are almost similar for 2 and 5 wt % of BSA. It would require the data in the much lower Q region to measure the sizes of the aggregates. SANS data of silica nanoparticle BSA were fitted by the fractal structure of the nanoparticle aggregates coexisting with the free proteins. The fractal dimension is found to be about 2.4 in all the aggregated nanoparticle systems.

We have, thus, shown that BSA, similar to lysozyme protein, induces the aggregation of silica nanoparticles through the different interaction mechanisms. The dominance of the attractive interaction over the repulsive interaction responsible for the aggregation of the nanoparticles for lysozyme and BSA is compared in Fig. 7. In the case of oppositely charged lysozyme, the aggregation arises as a result of charge neutralization on the nanoparticles and their bridging by the protein. The attractive interaction responsible for aggregation is found to be the short-range interaction. On the other hand, the aggregation of the nanoparticles in the presence of similarly charged silica nanoparticles and BSA (both anionic) is entropy driven. It arises because of nonadsorption of the BSA protein on the nanoparticles. This entropy driven attraction (depletion) is determined to be the long-range attraction.

V. CONCLUSIONS

Small-angle neutron scattering has been used to study the interaction of silica nanoparticles with lysozyme and BSA proteins. The measurements were carried out at a fixed concentration of silica nanoparticles and over a wide range of protein concentrations. It has been found that the phase behavior of the nanoparticle-protein system is highly affected by the type of protein and its concentration. The electrostatic interaction plays a crucial role in tuning the nanoparticle-protein interaction. In the case of the silica nanoparticle-lysozyme system, the protein adsorbs on the nanoparticle surface due to the electrostatic attractive interaction, which leads to protein-mediated aggregation, even for very small amounts of the protein. On the other hand, the nonadsorption of BSA on the nanoparticle surface due to the electrostatic repulsive interaction provides the depletion force. At high BSA concentrations, the domination of the depletion interaction over the electrostatic repulsion between nanoparticles results in the aggregation of the nanoparticles, similar to that with lysozyme. The aggregates, irrespective of protein type and concentration, are characterized by a fractal structure having a fractal dimension of 2.4.

[1] W. H. Suh, Y. H. Suh, and G. D. Stucky, Nano Today **4**, 27 (2009).
[2] H. Wu, D. Kong, Z. Ruan, P.-C. Hsu, S. Wang, Z. Yu, T. J. Carney, L. Hu, S. Fan, and Y. Cui, Nat. Nanotechnol. **8**, 421 (2013).
[3] R. Langer and D. A. Tirrell, Nature (London) **428**, 487 (2004).
[4] R. Thiruvengadathan, V. Korampally, A. Ghosh, N. Chanda, K. Gangopadhyay, and S. Gangopadhyay, Rep. Prog. Phys. **76**, 066501 (2013).

[5] I. Bernacka-Wojcik, P. Lopes, A. C. Vaz, B. Veigas, P. J. Wojcik, P. Simões, D. Barata, E. Fortunato, P. V. Baptista, H. Águas, and R. Martins, Biosens. Bioelectron. **48**, 87 (2013).

[6] H. Yuan, J. Li, G. Bao, and S. Zhang, Phys. Rev. Lett. **105**, 138101 (2010).

[7] T. Zhu, Z. Jiang, and Y. Ma, Appl. Phys. Lett. **102**, 153109 (2013).

[8] B. J. H. Fendler and F. C. Meldrum, Adv. Mater. **7**, 607 (1995).

[9] M. Mahmoudi, I. Lynch, M. R. Ejtehadi, M. P. Monopoli, F. B. Bombelli, and S. Laurent, Chem. Rev. **111**, 5610 (2011).

[10] M.-E. Aubin-Tam and K. Hamad-Schifferli, Biomed. Mater. **3**, 034001 (2008).

[11] J. Ge, J. Lei, and R. N. Zare, Nat. Nanotechnol. **7**, 428 (2012).

[12] K. Fan, C. Cao, Y. Pan, D. Lu, D. Yang, J. Feng, L. Song, M. Liang, and X. Yan, Nat. Nanotechnol. **7**, 459 (2012).

[13] F. Bai, C. Wang, Q. Lu, M. Zhao, F.-Q. Ban, D.-H. Yu, Y.-Y. Guan, X. Luan, Y.-R. Liu, H.-Z. Chen, and C. Fang, Biomaterials **34**, 6163 (2013).

[14] R. Chen, P. Choudhary, R. N. Schurr, P. Bhattacharya, J. M. Brown, and P. C. Ke, Appl. Phys. Lett. **100**, 013703 (2012).

[15] I. Lynch, T. Cedervall, M. Lundqvist, C. Cabaleiro-Lago, S. Linse, and K. A. Dawson, Adv. Colloid Interface Sci. **134–135**, 167 (2007).

[16] G. Orts-Gil, K. Natte, R. Thiermann, M. Girod, S. Rades, H. Kalbe, A. F. Thünemann, M. Maskos, and W. Österle, Colloids Surf., B **108**, 110 (2013).

[17] I. Lynch and K. A. Dawson, Nano Today **3**, 40 (2008).

[18] X. Yu, D. Y. Lei, F. Amin, R. Hartmann, G. P. Acuna, A. Guerrero-Martínez, S. A. Maier, P. Tinnefeld, S. Carregal-Romero, and W. J. Parak, Nano Today **8**, 480 (2013).

[19] H. He, X. Xu, H. Wu, Y. Zhai, and Y. Jin, Anal. Chem. **85**, 4546 (2013).

[20] M. Lundqvist, I. Sethson, and B.-H. Jonsson, Langmuir **20**, 10639 (2004).

[21] Y. Min, M. Akbulut, K. Kristiansen, Y. Golan, and J. Israelachvili, Nature Mater. **7**, 527 (2008).

[22] P. Roach, D. Farrar, and C. C. Perry, J. Am. Chem. Soc. **128**, 3939 (2006).

[23] A. A. Vertegal, R. W. Siegel, and J. S. Dordick, Langmuir **20**, 6800 (2004).

[24] F. Turci, E. Ghibaudi, M. Colonna, B. Boscolo, I. Fenoglio, and B. Fubini, Langmuir **26**, 8336 (2010).

[25] K. Rezwan, L. P. Meier, M. Rezwan, J. Voros, M. Textor, and L. J. Gauckler, Langmuir **20**, 10055 (2004).

[26] K. Rezwan, A. R. Studart, J. Voros, and L. J. Gauckler, J. Phys. Chem. B **109**, 14469 (2005).

[27] L. Wang, W. Zhao, and W. Tan, Nano Res. **1**, 99 (2008).

[28] K. Rezwan, L. P. Meier, and L. J. Gauckler, Biomaterials **26**, 4351 (2005).

[29] B. Bharti, J. Meissner, and G. H. Findenegg, Langmuir **27**, 9823 (2011).

[30] J. R. Lu, T. J. Su, R. K. Thomas, and J. Penfold, Langmuir **14**, 6261 (1998).

[31] J. Wang, U. B. Jensen, G. V. Jensen, S. Shipovskov, V. S. Balakrishnan, D. Otzen, J. S. Pedersen, F. Besenbacher, and D. S. Sutherland, Nano Lett. **11**, 4985 (2011).

[32] D. I. Svergun and M. H. J. Koch, Rep. Prog. Phys. **66**, 1735 (2003).

[33] G. D. Wignall and Y. B. Melnichenko, Rep. Prog. Phys. **68**, 1761 (2005).

[34] N. Osaka, H. Endo, T. Nishida, T. Suzuki, H.-J. Li, K. Haraguchi, and M. Shibayama, Phys. Rev. E **79**, 060801 (2009).

[35] S. Kumar and V. K. Aswal, J. Phys.: Condens. Matter. **23**, 035101 (2011).

[36] A. J. Chinchalikar, V. K. Aswal, J. Kohlbrecher, and A. G. Wagh, Phys. Rev. E **87**, 062708 (2013).

[37] S. Chodankar, V. K. Aswal, J. Kohlbrecher, R. Vavrin, and A. G. Wagh, J. Phys.: Condens. Matter **19**, 326102 (2007).

[38] J. Kohlbrecher and W. Wagner, J. Appl. Crystallogr. **33**, 804 (2000).

[39] J. B. Hayter and J. Penfold, Colloid Polym. Sci. **261**, 1022 (1983).

[40] J. S. Pedersen, Adv. Colloid Interface Sci. **70**, 171 (1997).

[41] S. Kumar, V. K. Aswal, and J. Kohlbrecher, Langmuir **28**, 9288 (2012).

[42] Y. Liu, E. Fratini, P. Baglioni, W.-R. Chen, and S.-H. Chen, Phys. Rev. Lett. **95**, 118102 (2005).

[43] Y. Liu, W.-R. Chen, and S.-H. Chen, J. Chem. Phys. **122**, 044507 (2005).

[44] J. Teixeira, J. Appl. Crystallogr. **21**, 781 (1988).

[45] J. S. Pedersen, J. Appl. Crystallogr. **24**, 893 (1991).

[46] P. R. Bevington, *Data Reduction and Error Analysis for Physical Sciences* (McGraw-Hill, New York, 1969).

[47] S. Kumar, V. K. Aswal, and J. Kohlbrecher, Langmuir **27**, 10167 (2011).

[48] A. Shukla, E. Mylonas, E. D. Cola, S. Finet, P. Timmins, T. Narayanan, and D. I. Svergun, Proc. Natl. Acad. Sci. USA **105**, 5075 (2008).

[49] A. Stradner, F. Cardinaux, and P. Schurtenberger, Phys. Rev. Lett. **96**, 219801 (2006).

[50] S. Kumar, M.-J. Lee, V. K. Aswal, and S.-M. Choi, Phys. Rev. E **87**, 042315 (2013).

[51] Y. Liu, L. Porcar, J. Chen, W.-R. Chen, P. Falus, A. Faraone, E. Fratini, K. Hong, and P. Baglioni, J. Phys. Chem. B **115**, 7238 (2011).

[52] S. Chodankar, V. K. Aswal, J. Kohlbrecher, R. Vavrin, and A. G. Wagh, Phys. Rev. E **79**, 021912 (2009).

[53] A. M. Yake, C. E. Snyder, and D. Velegol, Langmuir **23**, 9069 (2007).

[54] T. J. Su, J. R. Lu, R. K. Thomas, Z. F. Cui, and J. Penfold, J. Phys. Chem. B **102**, 8100 (1998).